Microfluid Nanofluid (2017) 21:119
DOI 10.1007/s10404-017-1954-z

SHORT COMMUNICATION

Geometry-confined bifurcation at low flow rate in flow-focusing droplet generator

Jie Wu[1] · Qifan Yan[1] · Yiwen Cui[1] · Shouhu Xuan[1] · Xinglong Gong[1]

Received: 7 March 2017 / Accepted: 21 June 2017

This communication describes the stable dripping (period-1)-bifurcation (period-2)-dripping (period-1) transition phenomenon in flow-focusing droplet generator. Different from the traditional higher-order periodic and chaotic bubbling which usually happened in the condition of high Weber number (*We*), this transition is acquired under low flow rate. Experimental observations demonstrate this transition strongly depends on the orifice length, which indicates that the combination of capillary pressure and inertia dominates this regime.

Microdroplet technology has been exploited in the last two decades to provide diverse applications, especially in the areas of chemistry and biology, for example, food processing (Maan et al. 2015), targeted drug delivery (Van Wamel et al. 2016), diagnostic testing (El-Ali et al. 2006), and particle synthesis (Baah and Floyd-Smith 2014). In all microdroplet generation techniques, flow focusing has been proven to be a very effective and broad-spectrum method for generating the droplets and bubbles (Anna et al. 2003; Garstecki et al. 2005b; Gulati et al. 2016; Tan et al. 2006; Woodward et al. 2007; Xu and Nakajima 2004). In principle, the flow-focusing method is based on a co-flow that contains inner and outer two-phase fluids, in which the inner phase is pinched off by the outer phase to release droplets through an orifice.

Owing to the extensive application of flow-focusing droplet generator, many groups have studied the breakup modes of droplet to guide the devices designation. As soon as Anna firstly described this complex process (Anna et al. 2003), various experiments, theories, and computations have been conducted to study these behaviors by changing geometry dimension (Gupta et al. 2014), fluids properties (Nie et al. 2008), flow rates (Garstecki et al. 2005b), and other parameters. Usually, droplet breakup regimes can be divided into squeezing, dripping, thread formation, and jetting (Lee et al. 2009). Though the monodisperse droplets are obtained in the above regimes, some polydispersity situations also exist. The most common one is dripping with satellite, a very small droplet induced by unbalance capillary force follows behind a primary droplet. Another case is the nonlinear phenomena in flow-focusing device including period-doubling, period-halving bifurcation, intermittency, and chaos (Garstecki et al. 2005a). Related nonlinear dynamic studies have been completed including nozzle injects (Liu et al. 2004), dripping faucet (Ambravaneswaran et al. 2000), and flow-focusing bubbling (Garstecki et al. 2005a). It was observed that the monodisperse bubbles or droplets were replaced by repeating sequences of two, four, or more fluid segments with different sizes when the flow rate of the dispersed phase or continuous phase exceeded a critical value. The period-n ($n = 1, 2, 3, 4\ldots$) was used to express the regimes of drop breakup, where n presented the branch number of droplet or bubble size. However, bifurcation almost happened under high flow rates in these studies. With the increase of the flow rate of inner phase or outer phase, the regimes changed from period 1–2–4… in turn.

In this communication, a stable period 1–2–1 transition under low flow rates was described. The nonlinear dynamics of flow-focusing bubble generator has been proved to be dominated by inertia (Garstecki et al. 2005a). We cannot help wondering whether the bifurcation under low flow rate is based on the same principle since the complex dripping behavior. Understanding the dynamics of this phenomenon

✉ Xinglong Gong
gongxl@ustc.edu.cn

[1] CAS Key Laboratory of Mechanical Behavior and Design of Materials, Department of Modern Mechanics, University of Science and Technology of China (USTC), Hefei 230027, China

Published online: 28 June 2017

can help to control the range of parameters and gain uniform fluid segment.

Figure 1a shows the flow-focusing devices used in the experiments. Devices with different orifice length (l_{or}) were prepared by standard soft lithography techniques (Coullet et al. 2004) to investigate the origination of the bifurcation. These two channels have a uniform height of $h = 72$ μm, the width of the inlet of dispersed phase $w_{din} = 200$ μm, continuous phase $w_{cin} = 217$ μm, orifice $w_{or} = 40$ μm, and the length of the orifice $l_{or} = 50$ μm for short orifice flow-focusing device (SFF) and 210 μm for long orifice flow-focusing device (LFF). Syringe pumps drove mineral oil as continuous phase and water as dispersed phase without any surfactant. An interface was formed between mineral oil and water at the cross-junction of the geometry. The oil flowed around the water during entering the orifice. Viscous and hydrostatic pressure together led the collapse of water thread. Interfacial tension kept the tip from moving forward. We marked the flow rate of mineral oil as Q_c and water as Q_d. At 25 °C, the density and viscosity of deionized water and mineral oil are 995 kg/m^3 and 1 mPa s, 817 kg/m^3 and 40 mPa s, respectively. The interfacial tension of the two immiscible fluids is 37.5 mN/m measured by pendant drop method. Figure 1b illustrates the volume of droplets as a function of Q_c when Q_d (200 μL/h) was a constant. All droplets in SFF were monodispersed as Q_c increased. While in LFF, monodispersed droplets (Fig. 1c) firstly turned to bifurcation (Fig. 1d, a primary droplet was followed by a relatively small secondary droplet), then the system produced identical droplets (Fig. 1e) again. In a particular Q_c range, the volume of droplets fluctuated with the increase of Q_c when Q_d fixed at 200 μL/h (Fig. 1b), which denoted the bifurcation regime in LFF device.

To investigate the formation process of the dripping–bifurcation–dripping transition in LFF device, detailed experiments were designed by increasing Q_c from 160 to 2000 μL/h and Q_d accordingly. For example, $Q_d = 160$, 80, …, 16 μL/h ($Q_c = 160$ μL/h) that meant the flow rate ratio (Q_c/Q_d) was increased from 1 to 10. Figure 2a shows the typical flow map which was based on the inlet capillary numbers of each fluids. Here the crucial superficial velocity of liquid and inlet capillary number are defined as $u_j = Q_j/w_{jin}h$, $Ca_{jin} = \eta_j u_j/\gamma$, respectively. The subscript "j"

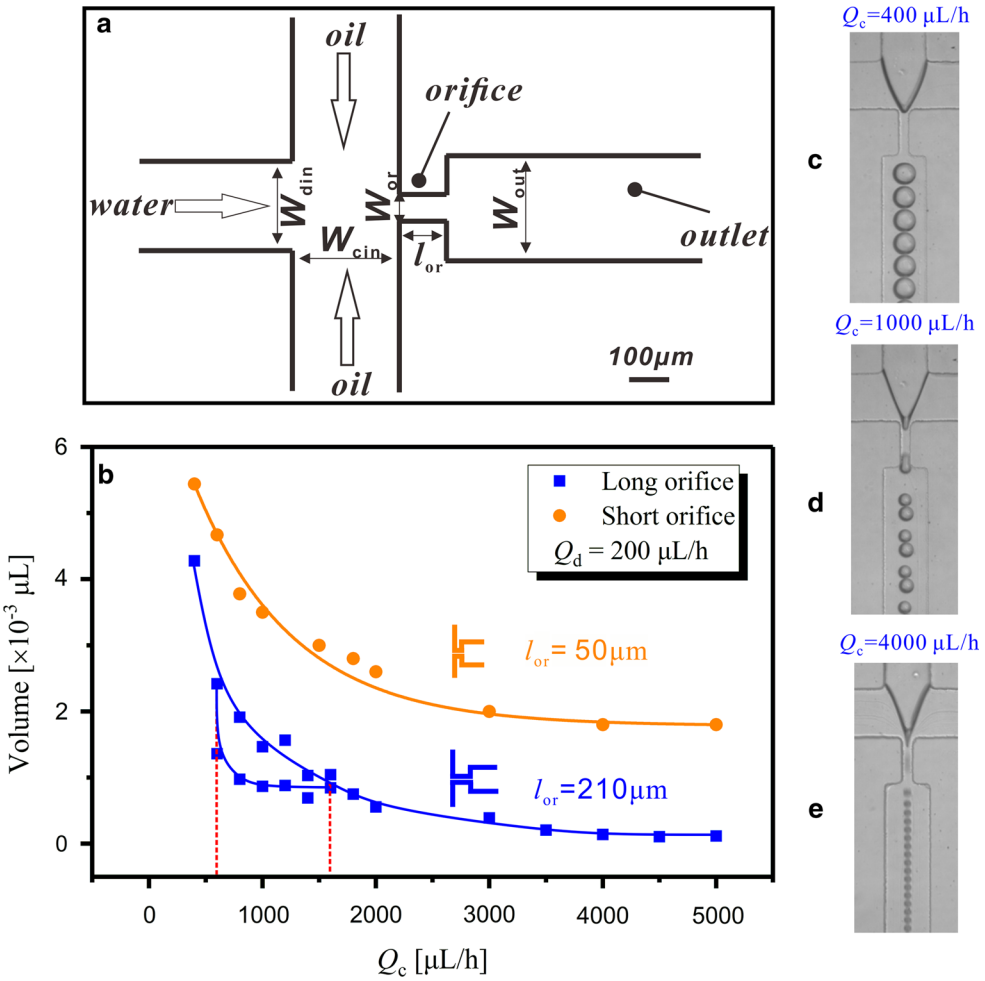

Fig. 1 **a** The plane sketch map of the flow-focusing geometry. The channels have a uniform height of $h = 72$ μm, the width of the inlet of dispersed phase and continuous phase, $w_{din} = 200$ μm and $w_{cin} = 217$ μm, the width of the orifice, $w_{or} = 40$ μm, the length of the orifice, $l_{or} = 50$ μm for SFF and 210 μm for LFF. **b** Droplets volume as a function of flow rate of continuous phase (Q_c) under fixed flow rate of dispersed phase ($Q_d = 200$ μL/h). For SFF geometry, all droplets generated in dripping area. For LFF geometry, dripping–bifurcation–dripping transition appeared. **c**, **d**, **e** The transition of LFF where Q_c increased from 400 to 4000 μL/h

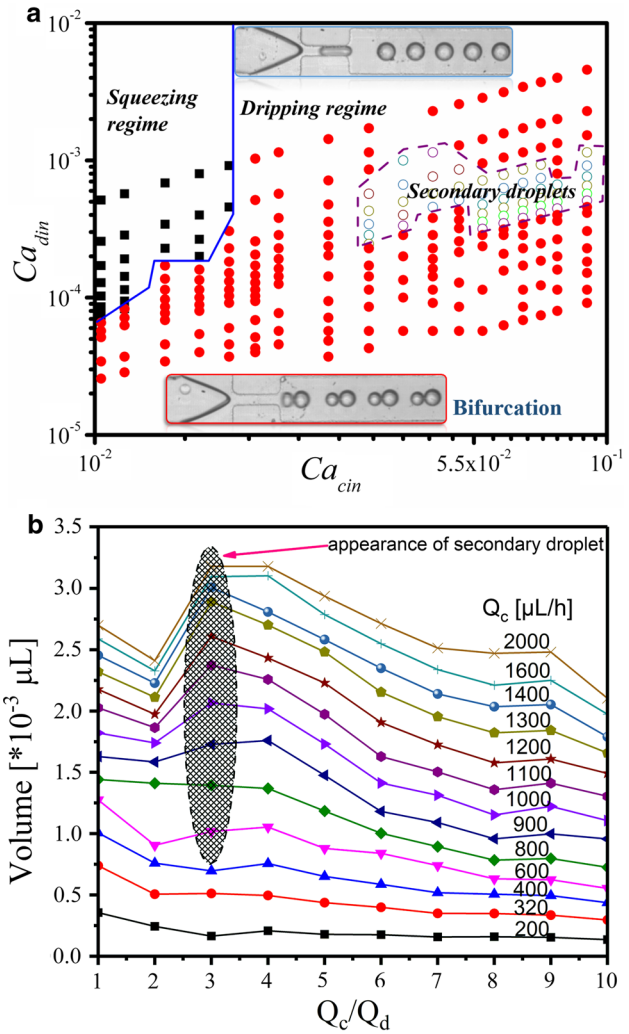

Fig. 2 **a** Flow map of LFF droplet generator about the inlet capillary number space of two phases (squeezing regime, dripping regime, and secondary droplets). The micrograph *insets* show the typical modes of the two regimes. Flow rate of continuous phase Q_c was taken from 200 to 2000 μL/h, and flow rate ratio Q_c/Q_d was chosen from 1 to 10. **b** Droplets volume versus Q_c/Q_d under various Q_c. Primary and secondary droplets were taken as a whole to calculate the volume for bifurcation. The *oval shadow area* indicates the appearance of secondary droplet

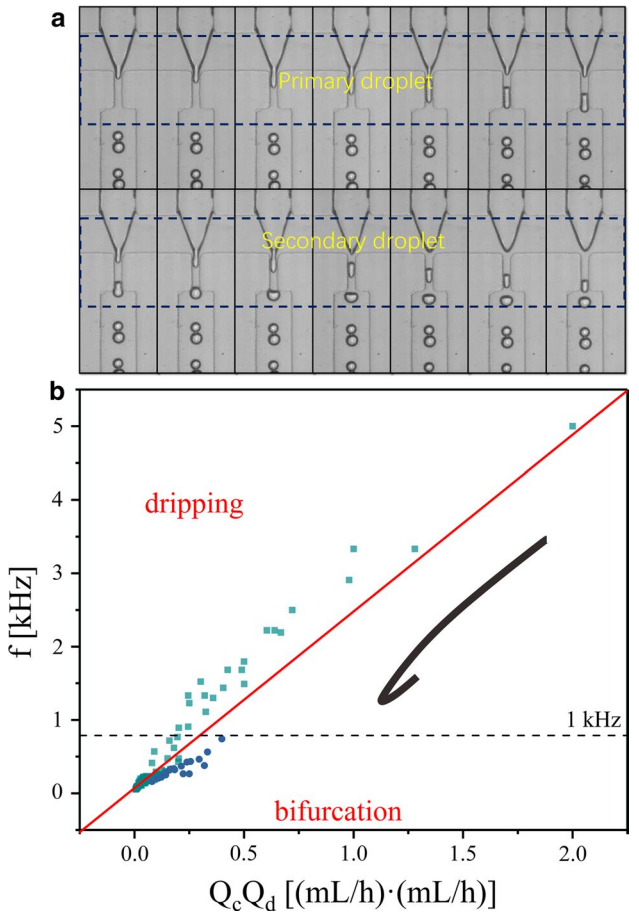

Fig. 3 **a** Breakup process of a pair of primary and secondary droplets. **b** Frequency of droplets plotted against the product (Q_cQ_d). Outline of novel frequency bifurcation is shown as the *solid line* (not to scale). The short arm represented bifurcation regime, and the long arm represented dripping regime

in the formulas can be divided into two cases, "*c*" (continuous phase) and "*d*" (dispersed phase). The subscript "*in*" means "inlet." η denotes viscosity of fluid, and γ is interfacial tension of two immiscible fluids. For example, Ca_{cin} means the inlet capillary number of continuous phase. The flow map showed a comprehensive dripping (period-1) regime with throughout $Ca_{din} < 10^{-2}$. When the value of Ca_{cin} was relatively low, the regime of the flow-focusing devices was squeezing or dripping (no secondary droplets) with Ca_{din} increasing. With the increase of Ca_{cin}, bifurcation (period-2) started to appear. At a particular Ca_{cin}, bifurcation only occurred within a certain Ca_{din} range. Figure 2b shows the droplets volume versus flow rate ratio when Q_c was kept as a constant. Primary and secondary droplets were considered as a whole here to calculate droplet volume. In general, droplet volume first decreased with increase in Q_c/Q_d. Then, a sudden increase in volume was found, which indicated the presence of secondary droplets. The shadow area in Fig. 2b showed that all bifurcation appeared when Q_c/Q_d was about 3. Actually, the bifurcation still existed when the value of Q_c exceeded 3000 μL/h. In conclusion, the flow map (Fig. 2a) and volume map (Fig. 2b) showed a minimal value of Ca_{cin} about 10^{-2} for the possibility of bifurcation. During the appearance of bifurcation, the Q_c/Q_d was around 3. Under these prerequisites, increasing Q_c or Q_d led to bifurcation.

In order to study the origination dynamics of secondary droplets, the micrographs of generation process were firstly focused (Fig. 3a). In each period, tip of dispersed phase began to grow and form a thread near the entrance of orifice. Hydrodynamic pressure, capillary stresses, viscous

forces, and inertia forces worked together to induce the breakup of primary droplet in the orifice. Primary droplet started to move along the orifice toward downstream. Before the primary droplet left the orifice, the tip grew again and a smaller secondary droplet was induced. There was no visible contraction of the tip in the generation gap of primary and secondary droplets. Then, the thread retracted and the sequence repeated.

It is important to determine the physical parameters that control the transition from dripping to bifurcation. A flow-focusing device is always divided into three parts: inlet channel, orifice, and outlet channel. Obviously, the occurrence of the bifurcation should be attributed to the dynamics of the thread in the part of orifice and has nothing to do with the entrances and the outlet. The micrographs (Fig. 3a) of breakup process manifested that no perturbation was occurred during the formation of primary and secondary droplets. During the formation of the secondary droplet, the primary droplet was still within (or close to) the orifice. Therefore, the evolution of two immiscible phase interface in the orifice was crucial. The frequency f of droplet breakup was introduced to study the interface. There is also a bifurcation of frequency (f) relative to the product of Q_c and Q_d (Fig. 3b). The product of Q_c and Q_d (like *We*'s "u^2") was used to consider the combined effect of flow rate of dispersed phase and continuous phase. The long arm represented dripping regime, and the short arm represented bifurcation regime. Frequency of the bifurcation regime was always below the critical value of $f_{cr} = 1$ kHz, which indicated this bifurcation occurred at a relatively low frequency.

The dimensionless parameter capillary number (*Ca*) and Weber number (*We*) are used to characterize the relative effects of viscous forces and inertia forces on interfacial tension. To analyze the flow condition in the orifice, Ca_{flow} and We_{flow}, calculated on the basis of the mean speed of the liquid through the orifice, were introduced to compare the viscous and the inertial term exerted on the interface of growing thread and continuous phase of the flowing liquids with capillary pressure. Ca_{intfc} and We_{intfc}, calculated on the basis of the frequency of droplet generation and the typical length scale of the evolution of the water–oil interface, were introduced to distinguish the shear stresses and inertial term exerted on the interface of recoil tip and continuous phase counteracting the capillary pressure.

The mean speed of the liquid through the orifice is $u_{flow} = Q/w_{or}h$ ($Q = Q_c + Q_d$, $w_{or} = 40$ μm, $h = 72$ μm, shown in Fig. 1a). Thus, $Ca_{flow} = \mu u_{flow}/\gamma$ and $We_{flow} = \rho u_{flow}^2 h/\gamma$ ($\mu = 40$ mPa s, $\rho = 817$ kg/m^3, $\gamma = 37.5$ mN/m). In our experimental flow rates range, $Ca_{flow} \in (10^{-2}, 10^{-1})$, the shear stress acting on the interface of liquids has little effect on its shape. Also, $We_{flow} \in (10^{-4}, 10^{-1})$ indicated regimes were dominated by interfacial tension. The typical speed of the interface was calculated as $u_{intfc} \approx l_{or}f$. The characteristic length scale for evolution of the tip was on the order of w_{or}. These estimates were used to calculate $Ca_{intfc} = \mu u_{intfc}/\gamma$ and $We_{intfc} = \rho u_{intfc}^2 w_{or}/\gamma$ which obtained $Ca_{intfc} \in (10^{-2}, 1)$ and $We_{intfc} \in (10^{-4}, 1)$. The values suggested that viscous and inertia forces were not dominated by capillary pressure. With increase in the flow rate, both viscous and inertial effects tended to play the dominant role. As a result, (Ca_{flow}, We_{flow}) and (Ca_{intfc}, We_{intfc}) showed interfacial tension dominated the dynamics of both droplets breakup and the relaxation of the interface. This is the so-called bifurcation under low flow rate, which is different from the dripping faucet (Ambravaneswaran et al. 2000) or the inverted dripping faucet (Garstecki et al. 2005a).

Compared LFF with SFF, it was found that the longer orifice induced higher frequency of droplets generation, which indicated faster interface velocity and higher *We*. In this sense, inertial term led to the bifurcation, just like the mechanism of inverted dripping faucet (Garstecki et al. 2005a). However, according to the non-dimensional parameter analysis, interfacial tension occupied the dominant position. As a result, the capillary pressure and inertia worked together to induce the secondary droplets under low flow rate within a certain range (low value of Q_cQ_d less than 0.5, Fig. 3b). As the flow rates continued to increase, shear stress was firstly dominated, which led to dripping regime again. Then, inertia and interfacial tension exceeded the other factors; nonlinear phenomenon appeared.

A novel secondary droplet phenomenon under low flow rate was studied in this communication. Unlike the traditional high-order nonlinear phenomenon, this regime presented period 1–2–1 transition. Flow-focusing droplet generator with long orifice tended to induce this transition, while the short orifice geometry was attributed to a different manner. Appearance of bifurcation under low flow rate was dominated by interfacial tension, and it was further strongly influenced by inertial term.

Acknowledgements Financial supports from the National Natural Science Foundation of China (Grant Nos. 11572310, 11572309) are gratefully acknowledged. This study was also supported by the Collaborative Innovation Center of Suzhou Nano Science and Technology. This work was partially carried out at the USTC Center for Micro and Nanoscale Research and Fabrication.

References

Ambravaneswaran B, Phillips SD, Basaran OA (2000) Theoretical analysis of a dripping faucet. Phys Rev Lett 85:5332

Anna SL, Bontoux N, Stone HA (2003) Formation of dispersions using "flow focusing" in microchannels. Appl Phys Lett 82:364–366

Baah D, Floyd-Smith T (2014) Microfluidics for particle synthesis from photocrosslinkable materials. Microfluid Nanofluid 17:431–455

Coullet P, Mahadevan L, Riera C (2004) Hydro-dynamical models for the chaotic dripping faucet. arXiv preprint physics/0408096

El-Ali J, Sorger PK, Jensen KF (2006) Cells on chips. Nature 442:403–411

Garstecki P, Fuerstman MJ, Whitesides GM (2005a) Nonlinear dynamics of a flow-focusing bubble generator: an inverted dripping faucet. Phys Rev Lett 94:234502

Garstecki P, Stone HA, Whitesides GM (2005b) Mechanism for flow-rate controlled breakup in confined geometries: a route to monodisperse emulsions. Phys Rev Lett 94:164501

Gulati S, Vijayakumar K, Good WW, Tamayo WL, Patel AR, Niu X (2016) Microdroplet formation in rounded flow-focusing junctions. Microfluid Nanofluid 20:2

Gupta A, Matharoo HS, Makkar D, Kumar R (2014) Droplet formation via squeezing mechanism in a microfluidic flow-focusing device. Comput Fluids 4(100):218–226

Lee W, Walker LM, Anna SL (2009) Role of geometry and fluid properties in droplet and thread formation processes in planar flow focusing. Phys Fluids 21:032103

Liu M-Y, Hu Z-D, Li J-H (2004) Multi-scale characteristics of chaos behavior in gas–liquid bubble columns. Chem Eng Commun 191:1003–1016

Maan AA, Nazir A, Khan MKI, Boom R, Schroën K (2015) Microfluidic emulsification in food processing. J Food Eng 147:1–7

Nie Z, Seo M, Xu S, Lewis PC, Mok M, Kumacheva E, Whitesides GM, Garstecki P, Stone HA (2008) Emulsification in a microfluidic flow-focusing device: effect of the viscosities of the liquids. Microfluid Nanofluid 5:585–594

Tan Y-C, Cristini V, Lee AP (2006) Monodispersed microfluidic droplet generation by shear focusing microfluidic device. Sens Actuators B 114:350–356

Van Wamel A, Healey A, Sontum PC, Kvåle S, Bush N, Bamber J, de Lange Davies C (2016) Acoustic cluster therapy (ACT)—preclinical proof of principle for local drug delivery and enhanced uptake. J Control Release 224:158–164

Woodward A, Cosgrove T, Espidel J, Jenkins P, Shaw N (2007) Monodisperse emulsions from a microfluidic device, characterised by diffusion NMR. Soft Matter 3:627–633

Xu Q, Nakajima M (2004) The generation of highly monodisperse droplets through the breakup of hydrodynamically focused microthread in a microfluidic device. Appl Phys Lett 85:3726–3728